

ELECTRON-ION EQUILIBRATION IN NONRADIATIVE SHOCKS ASSOCIATED
WITH SN 1006

J. MARTIN LAMING

SFA Inc., 1401 McCormick Drive, Landover, MD 20785¹

JOHN C. RAYMOND AND BRENDAN M. McLAUGHLIN

Harvard-Smithsonian Center for Astrophysics, 60 Garden Street, Cambridge, MA 02138

AND

WILLIAM P. BLAIR

Department of Physics and Astronomy, Johns Hopkins University, Baltimore, MD 21218

Received 1996 February 20; accepted 1996 June 5

ABSTRACT

The ultraviolet spectrum of SN 1006 observed by the Hopkins Ultraviolet Telescope (HUT) is modeled to infer the degree of electron-ion equilibration at the nonradiative shocks in the remnant. Such an approach is possible since the spectrum has lines (He II $\lambda 1640$) whose excitation is dominated by electrons, and others (C IV $\lambda 1550$, N V $\lambda 1240$, O VI $\lambda 1036$) in which protons and other ions are more important, and the intensity ratio between these is sensitive to the electron-ion temperature ratio. We find substantially less than full equilibration, marginally consistent with existing plasma simulations but rather more suggestive of even lower equilibration than these studies would predict. The more stringent limits on the electron temperature resulting from this allow a more accurate determination of the distance to SN 1006. Our result is 1.8 ± 0.3 kpc.

Subject headings: atomic processes — ISM: individual (SN 1006) — shock waves — supernova remnants

1. INTRODUCTION

A continuing open question in the physics of non-radiative shock fronts observed in young supernova remnants (SNRs) is the manner by which electron heating occurs directly behind the shock. In a nonradiative shock (so called because the power lost by radiation is dynamically unimportant), the temperature T deduced from the jump conditions for a distribution of particles with mass m is given by

$$kT = \frac{3}{16} m v_s^2, \quad (1)$$

where v_s is the shock velocity and k is Boltzmann's constant. Thus, in a hydrogen plasma the protons may have a temperature higher than the electrons by a factor 1836, the corresponding mass ratio. Other ions in the plasma might have even higher temperatures due to their greater masses. Once shocked, these various particle distributions will equilibrate by Coulomb collisions. Such equilibration will take place on a timescale that can be longer than the age of the SNR, leaving room for speculation that other mechanisms might be at work that could equalize electron and proton/ion temperatures at a much faster rate.

A simulation of a fast collisionless shock has been performed by Cargill & Papadopoulos (1988, hereafter CP), for the case of a quasi-perpendicular shock, i.e., with the shock velocity directed across the ambient magnetic field, with discussion also of extrapolation to the higher Mach numbers for SNRs. In the shock rest frame, ions reflected from the shock move upstream against the incoming ambient flow. For relative velocities ($\sim 2v_s$) greater than the electron thermal velocity [$v_e = (2kT/m_e)^{1/2}$], the Buneman instability (Buneman 1958) is excited, which heats the electrons to a temperature $kT \simeq 2m_e v_s^2$, about a factor of 10

greater than the temperature expected from the jump conditions, at which point the condition for the Buneman instability ceases to be satisfied. At this point, the ion-acoustic instability may switch on. The simulation of CP gives final electron temperatures about 300 times those expected from the jump conditions, which corresponds to about 20% of the shock energy going into heating electrons. In the absence of reflected ions, one might still expect a Buneman instability giving some electron heating behind the shock. For suitably high Mach numbers, the bulk velocity of the shocked plasma can be greater than the unshocked electron thermal velocity. However, the ensuing ion acoustic instability will be suppressed since the condition $T_e \gg T_i$ will not be satisfied behind the shock.

An alternative scenario has been presented by Lesch (1990), also for quasi-perpendicular shocks, whereby electrons drifting relative to ions across the magnetic field in the shock ramp excite lower hybrid waves, whose anomalous resistivity provides strong electron heating. In addition, ions reflected back upstream can excite ion plasma waves. Both these instabilities have significantly smaller growth rates for typical SNR conditions than those invoked by CP, but it is assumed that the reflected ion drift velocity will never exceed the electron thermal velocity. The electron temperatures found by Lesch (1990) appear to be somewhat higher, closer to the proton temperatures than the CP simulation.

Quasi-parallel shock simulations exist only for low Mach number shocks appropriate for the solar wind (Quest et al. 1983). Here, strong ion heating is attributed to whistler turbulence and is similar to that found for quasi-perpendicular shock simulations for equal electron and ion temperatures in the upstream plasma (Forslund et al. 1984). However, the electron heating for the parallel case is rather less than for the perpendicular case, which appears similar in magnitude relative to the ion temperature to the CP prediction above.

¹ Also Naval Research Laboratory, Code 7674L, Washington, DC 20375.

A certain amount of support for these simulations comes from observations of collisionless shocks in the solar wind by spacecraft flying through the shock itself (e.g., Scudder et al. 1986a, 1986b, 1986c). Electron plasma oscillations, ion-acoustic waves, lower hybrid waves, and whistlers have all been identified, along with magnetic and electric fields, current densities, and hence anomalous resistivities that might result from these plasma excitations.

In this paper we attempt a completely different test of such theoretical predictions, using an ultraviolet spectrum of a nonradiative shock filament in the young galactic supernova remnant SN 1006, obtained with the Hopkins Ultraviolet Telescope (HUT) during the Astro-2 space shuttle mission in 1995 March (see Raymond, Blair, & Long 1995). SN 1006 is one of only a handful of “historical” supernova remnants, the supernova having been observed by Chinese astronomers (see Clark & Stephenson 1977). The only known optical emission from the remnant arises from a faint filament on the northwest limb that shows a pure Balmer line optical spectrum, indicative of a collisionless shock encountering partially neutral preshock gas (Chevalier, Kirshner, & Raymond 1980). The velocity of these shocks is constrained by the optical spectra of the H α profile to be in the range 2200–3500 km s⁻¹ (Smith et al. 1991). The dominant uncertainty in this number comes from our lack of knowledge of the degree of electron-ion equilibration behind the shock. An unequilibrated plasma would suggest shock velocities toward the lower end of this range, whereas completely equilibrated plasmas would lead us to infer velocities at the higher end. More recent work (Smith, Laming, & Raymond 1996) suggests that the plasma is more or less unequilibrated, implying the lower shock velocities. It is important to determine the actual velocity of the shock as accurately as possible because, with the observed proper motion of the optical filament from Long, Blair, & van den Bergh (1988), an accurate distance to this important object can be derived.

The SN 1006 observations, reduction procedures, and preliminary interpretation are described by Raymond et al. (1995). Briefly, emission lines of H I (Ly β), He II λ 1640, and the resonance doublets of the Li-like ions C IV, N V, and O VI were observed. Emission-line widths are consistent with the \sim 2300 km s⁻¹ width reported for the broad component of H α (Smith et al. 1991). The immediate implication of this is that the emitting ions do not have the same temperature but appear to have the same velocity distributions, suggesting that no equilibration between the various ions and protons has taken place. Although the equilibration timescales based on Coulomb collisions would therefore predict no electron-ion equilibration also, we cannot draw this conclusion so straightforwardly because as discussed above, the plasma instabilities preferentially heat the electrons.

In § 2 we describe the atomic processes relevant to the observed UV emission, and in § 3 the computation of various shock models using these processes is outlined. Section 4 gives a discussion of the results of these models, together with improved determinations of the shock velocity and distance to SN 1006.

2. ATOMIC PROCESSES

For shock velocities in the range 2200–3500 km s⁻¹, equation (1) gives temperatures of order \sim 10⁸ K for protons and \sim 10⁵ K for the electrons. Following equi-

bration, both particle distributions will have temperatures about half the unequilibrated proton temperature. At these temperatures, the usual electron impact excitation and ionization processes will be important for all ions under consideration. However, for the Li-like resonance lines, it is likely that proton impact excitation will be important as well. Proton impact cross sections in general reach their maxima at an incident proton velocity comparable to the electron velocity that corresponds to the excitation or ionization threshold energy. Hence, the maxima in the Li-like resonance line proton impact excitation cross sections (thresholds \sim 10 eV) will be at proton energies of 15–20 keV. The maxima for excitation of He II λ 1640 (threshold \sim 48 eV) or for ionization of He II or the Li-like ions (thresholds $>$ 54 eV) will be at proton energies about 100 keV or greater. At temperatures around 10⁸ K, it is clear that a substantial fraction of protons excite the Li-like ions very effectively, and as such they must be considered along with the usual electron impact processes.

However, assuming the proton impact ionization cross sections to be similar to those for electron impact ionization (Crandall et al. 1979) modified by their differing velocities (giving the proton cross section a higher maximum than for electrons), we estimate proton impact ionization rates for these ions at these temperatures to be 10% or less of the electron impact ionization rates. This is because the post-shock proton energies are all on the steeply rising low-energy part of the ionization cross section. Therefore, we neglect these processes hereafter. We note also that in forming the ratio of photons emitted per ion going through the shock, the proton contributions to the numerator and denominator of this fraction for He II (the ion with the lowest energy thresholds for neglected processes) will be similar because ionization and excitation processes have similar energy thresholds. Thus, the numerator and denominator will be affected by the same factor, leaving the ratio unchanged to first order. Similar arguments hold for excitation and ionization by alpha particles, and these excitation rates for Li-like ions are also included in the models, along with charge exchange ionization of neutral H by alpha particles. Collisions with He⁺ are neglected because the extra effect of these on the proton collision rates is less than the probable errors in these rates.

2.1. Proton and Alpha-Particle Excitation Rates

We have calculated heavy particle excitation cross sections for the Li-like resonance lines using a method based on the semiclassical analysis of Seaton (1964). In the Coulomb-Born approximation without exchange, the impact excitation cross section for dipole transitions is given in atomic units by (Burgess, Hummer, & Tully 1970, hereafter BHT)

$$\sigma = \frac{16\pi}{k_i^2} \frac{1}{(2l_a + 1)} \sum_{LL'} (2L + 1) \left| \begin{Bmatrix} L & l_a & l' \\ 1 & l & l_a \end{Bmatrix} \right|^2 \times \max(l, l') \max(l_a, l'_a) |D|^2, \quad (2)$$

where

$$D = \int_0^\infty F_{k_f}(r_2) \left[\int_0^{r_2} \psi_{n',l_a'}(r_1) \frac{r_2}{r_1} \psi_{n,l_a}(r_1) dr_1 + \int_{r_2}^\infty \psi_{n',l_a'}(r_1) \frac{r_1}{r_2} \psi_{n,l_a}(r_1) dr_1 \right] F_{k_i}(r_2) dr_2. \quad (3)$$

In equations (2) and (3), l and l_a are the initial orbital angular momenta of the free proton and bound electrons, respectively; the primed quantities are the final angular momenta. L is the total orbital angular momentum of the proton-ion system, which is necessarily conserved. The initial and final scattering particle wavevectors are denoted by k_i and k_f , respectively. F_{k_i}/r and F_{k_f}/r are initial and final Coulomb continuum radial wave functions for scattered proton, and $\psi_{n,l_a}/r$ and $\psi_{n',l'_a}/r$ are initial and final radial wave functions for the bound electrons. The quantity in braces in equation (2) is the Wigner six- j symbol. To simplify the calculation further, we let $r_2 \rightarrow 0$ in the limits of the integrals over r_1 (the Coulomb-Bethe approximation), which allows us to write

$$D = \int_0^\infty F_{k_f}(r_2) \frac{1}{r_2} F_{k_i}(r_2) dr_2 \times \int_0^\infty \psi_{n',l'_a}(r_1) r_1 \psi_{n,l_a}(r_1) dr_1. \quad (4)$$

The first integral is evaluated using formulae from the Appendix of BHT, modified for our case of a repulsive Coulomb field (see Alder et al. 1956), and the second integral is just the dipole matrix element. As it stands, such an approximation will seriously overestimate the cross section for low partial waves in which the projectile can penetrate the target. To remedy this, we use a procedure devised by Seaton (1964) whereby if the probability for the induced transition calculated in the above Coulomb-Bethe approximation exceeds 0.5, we set it equal to 0.5. We sum up explicitly over partial waves until we reach the angular momentum at which the calculated transition probability falls below 0.5, whereupon we complete the sum to $l = \infty$ using the Burgess sum rules (Burgess 1974) for the Coulomb-Bethe approximation. In checks of cross sections resulting from our method against the close-coupling calculations for $2s-2p$ dipole transitions in hydrogenic ions excited by proton impact of Zygelman & Dalgarno (1987), excellent agreement (to better than 10%) was found. The data used and resulting cross sections for C IV, N V, and O VI are given in Tables 1 and 2, in atomic units. The atomic unit of area is $a_0^2 = 2.798 \times 10^{-17} \text{ cm}^2$, and that of energy is 27.21 eV, or 2 ryd. Similar methods for calculating proton impact excitation cross sections are described by Walling & Weisheit (1988), where many other comparisons of related semiclassical calculations with the results of full quantum mechanical codes are described.

In the case of an SNR shock in which the plasma may not be in equilibrium, extra care is needed in evaluating the excitation rates from the cross sections. In general, one must perform a six-dimensional integral over the velocity distributions of both particles. Doing the angular parts analytically reduces this to a two-dimensional integral that can be evaluated numerically. In the usual case of electron impact excitation in thermal equilibrium, it may be

TABLE 1
EXCITATION POTENTIALS AND DIPOLE MATRIX
ELEMENTS FOR LI-LIKE IONS
(in Atomic Units)

Parameter	C IV	N V	O VI
ΔE	0.29	0.37	0.44
$ \langle 2s r 2p \rangle ^2$	1.48	0.952	0.67

TABLE 2

HEAVY PARTICLE IMPACT EXCITATION CROSS SECTIONS FOR LI-LIKE $2s-2p$ TRANSITIONS (in Atomic Units)

ENERGY (keV)	PROTONS			ALPHA PARTICLES		
	C IV	N V	O VI	C IV	N V	O VI
0.816.....	6.62
1.36.....	8.67	5.27	3.62
2.72.....	11.6	7.15	4.99
5.44.....	14.1	8.77	6.16
13.6.....	15.3	9.59	6.76
27.2.....	13.8	8.70	6.14	25.4	15.8	11.2
54.4.....	10.7	6.81	4.80	29.5	18.4	13.0
136.....	6.44	4.11	2.90	30.6	19.2	13.6
272.....	4.03	2.57	1.82	26.0	16.4	11.6
544.....	2.40	1.54	1.08	19.3	12.3	8.62
1360.....	1.17	0.74	0.53	12.8	8.22	5.84
2720.....	0.67	0.41	0.30	6.88	4.29	3.10
27200.....	0.086	0.054	0.038
108800.....	0.34	0.22	0.15

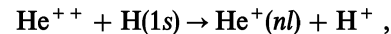
assumed that the ion is at rest, leaving a one-dimensional integral, but here we are dealing with protons and alpha particles, not electrons, and so the ionic motions may not be neglected so easily.

The excitation rate may then be written

$$C = 4\pi \left(\frac{m_1}{2\pi k T_1} \right)^{3/2} 4\pi \left(\frac{m_2}{2\pi k T_2} \right)^{3/2} \times \int_0^\infty \int_0^\infty \sigma(|\mathbf{v}_1 - \mathbf{v}_2|) |\mathbf{v}_1 - \mathbf{v}_2| v_1^2 v_2^2 \times \exp \left(-\frac{m_1 v_1^2}{2k T_1} \right) \exp \left(-\frac{m_2 v_2^2}{2k T_2} \right) dv_1 dv_2, \quad (5)$$

with m_i , v_i , and T_i being the mass, velocity, and temperature for particles of type i . Putting $|\mathbf{v}_1 - \mathbf{v}_2| \simeq (v_1^2 + v_2^2)^{1/2}$, we evaluate the expression for C numerically. Results for excitation rates for the Li-like ions for a suitable range of shock velocities are given for C IV, N V, and O VI for protons and alpha particles in Tables 3, 4, 5, 6, 7, and 8, respectively, in units of $10^{-8} \text{ cm}^3 \text{ s}^{-1}$.

The proton rates for H were taken from Smith, Laming, & Raymond (1996). Charge exchange rates for the processes



were taken from Hose (1995) for $nl = 3s, 3p, 3d$ and for the complete charge exchange cross section summed over all

TABLE 3
PROTON EXCITATION RATE COEFFICIENTS FOR C IV $2s-2p$

T_p (keV)	$C[T_i = (m_i/m_p)^a T_p] (10^{-8} \text{ cm}^3 \text{ s}^{-1})$				
	$a = 0$	$a = 0.25$	$a = 0.5$	$a = 0.75$	$a = 1.0$
1.36.....	1.8	1.9	2.1	2.5	3.0
2.04.....	2.5	2.6	2.9	3.3	4.0
2.72.....	3.1	3.3	3.6	4.1	4.9
4.08.....	4.1	4.3	4.7	5.3	6.1
5.44.....	4.9	5.1	5.5	6.1	6.9
6.80.....	5.5	5.7	6.1	6.7	7.5
8.16.....	6.0	6.2	6.7	7.3	8.0
10.88.....	6.8	7.1	7.5	8.0	8.7
13.60.....	7.4	7.6	8.1	8.6	9.0
16.32.....	7.8	8.1	8.4	8.9	9.2
19.04.....	8.1	8.4	8.7	9.1	9.3
21.76.....	8.4	8.6	8.9	9.2	9.3
24.48.....	8.5	8.8	9.0	9.2	9.3
27.20.....	8.6	8.9	9.1	9.3	9.4

TABLE 4
PROTON EXCITATION RATE COEFFICIENTS FOR N v 2s-2p

T_p (keV)	$C[T_i = (m_i/m_p)^a T_p] (10^{-8} \text{ cm}^3 \text{ s}^{-1})$				
	$a = 0$	$a = 0.25$	$a = 0.5$	$a = 0.75$	$a = 1.0$
1.36	1.1	1.2	1.3	1.5	1.9
2.04	1.5	1.6	1.8	2.1	2.5
2.72	1.9	2.0	2.2	2.6	3.1
4.08	2.5	2.7	2.9	3.3	3.8
5.44	3.0	3.2	3.4	3.8	4.3
6.80	3.4	3.6	3.8	4.2	4.7
8.16	3.7	3.9	4.1	4.5	5.1
10.88	4.2	4.4	4.7	5.0	5.5
13.60	4.6	4.8	5.0	5.4	5.7
16.32	4.9	5.0	5.3	5.6	5.8
19.04	5.1	5.2	5.5	5.7	5.8
21.76	5.2	5.4	5.6	5.8	5.9
24.48	5.4	5.5	5.7	5.8	5.9
27.20	5.4	5.6	5.7	5.9	5.9

final states of the He^+ ion. For the complete cross section, a couple of extra points at low energy were added from Hatton, Lane, & Winter (1979). High-energy points were taken from the asymptotic expressions provided by Briggs & Dubé (1980) for the $n = 3$ levels, and from Dubé & Briggs (1981) for the complete cross section. Charge exchange rates

TABLE 5
PROTON EXCITATION RATE COEFFICIENTS FOR O VI 2s-2p

T_p (keV)	$C[T_i = (m_i/m_p)^a T_p] (10^{-8} \text{ cm}^3 \text{ s}^{-1})$				
	$a = 0$	$a = 0.25$	$a = 0.5$	$a = 0.75$	$a = 1.0$
1.36	0.76	0.82	0.90	1.1	1.3
2.04	1.1	1.1	1.2	1.5	1.8
2.72	1.4	1.4	1.6	1.8	2.2
4.08	1.8	1.9	2.0	2.3	2.7
5.44	2.1	2.2	2.4	2.7	3.1
6.80	2.4	2.5	2.7	3.0	3.3
8.16	2.6	2.7	2.9	3.2	3.6
10.88	3.0	3.1	3.3	3.5	3.9
13.60	3.2	3.3	3.5	3.8	4.0
16.32	3.4	3.5	3.7	3.9	4.1
19.04	3.6	3.7	3.8	4.0	4.1
21.76	3.7	3.8	3.9	4.1	4.1
24.48	3.8	3.8	4.0	4.1	4.1
27.20	3.8	3.9	4.0	4.1	4.2

TABLE 6
ALPHA-PARTICLE EXCITATION RATE COEFFICIENTS FOR C IV 2s-2p

T_α (keV)	$C[T_i = (m_i/m_p)^a T_p] (10^{-8} \text{ cm}^3 \text{ s}^{-1})$				
	$a = 0$	$a = 0.25$	$a = 0.5$	$a = 0.75$	$a = 1.0$
5.44	2.5	2.7	3.1	3.6	4.2
8.16	4.1	4.5	5.1	5.7	6.5
10.88	5.7	6.2	6.8	7.5	8.3
16.32	8.3	8.9	9.5	10.4	11.4
21.76	10.3	10.9	11.7	12.6	13.7
27.20	12.0	12.6	13.5	14.5	15.6
32.64	13.4	14.2	15.1	16.1	17.3
43.52	16.0	16.8	17.7	18.8	19.9
54.40	15.5	18.7	19.6	20.6	21.1
65.28	19.4	20.2	21.0	21.9	22.6
76.16	20.5	21.3	22.0	22.4	23.4
87.04	21.4	22.1	22.8	23.5	23.9
97.92	22.2	22.8	23.1	23.9	24.4
108.80	22.9	23.3	23.9	24.3	24.8

TABLE 7
ALPHA-PARTICLE EXCITATION RATE COEFFICIENTS FOR N v 2s-2p

T_α (keV)	$C[T_i = (m_i/m_p)^a T_p] (10^{-8} \text{ cm}^3 \text{ s}^{-1})$				
	$a = 0$	$a = 0.25$	$a = 0.5$	$a = 0.75$	$a = 1.0$
5.44	1.5	1.6	1.9	2.2	2.6
8.16	2.5	2.7	3.1	3.5	4.0
10.88	3.4	3.7	4.1	4.6	5.2
16.32	5.0	5.4	5.8	6.4	7.1
21.76	6.3	6.6	7.1	7.8	8.6
27.20	7.3	7.7	8.3	9.0	9.8
32.64	8.2	8.7	9.3	10.0	10.9
43.52	9.8	10.3	11.0	11.7	12.5
54.40	9.6	9.8	12.2	12.9	13.3
65.28	12.0	12.5	13.1	13.7	14.3
76.16	12.7	13.2	13.8	14.0	14.7
87.04	13.3	13.7	14.2	14.6	15.1
97.92	13.7	14.2	14.6	15.0	15.4
108.80	14.2	14.6	14.9	15.3	15.7

with fast neutral H were computed using equation (5) above, while those with slow neutral H diffusing through the shock were calculated using equation (10) of Laming (1990) for a shock velocity of 2600 km s^{-1} (bulk velocity of 1950 km s^{-1}).

2.2. Electron Excitation and Ionization Rates

The electron excitation rates for the Li-like ions were taken from the distorted wave calculations of J. Mann (Magee et al. 1977). These may be less accurate than more recent calculations near threshold, but for these models we are more interested in correct behavior far above threshold. The cross sections were fitted to a form that ensures that they approach the correct high-energy asymptotic behavior. The ionization rates for all elements were taken from Arnaud & Rothenflug (1985).

The electron impact excitation rates for He^+ required a surprisingly large effort due to discrepancies among values in the literature and the need for rates at temperatures far above those considered in works such as Aggarwal et al. (1992) and Berrington, Kisielius, & Norrington (1996) at which $T \leq 5 \times 10^5 \text{ K}$. We have obtained electron impact excitation rates for He^+ from a 21 state *R*-matrix calculation, 15 for the *LS* levels through $n = 5$ and 6 pseudo-states to represent higher n and continuum states

TABLE 8
ALPHA-PARTICLE EXCITATION RATE COEFFICIENTS FOR O VI 2s-2p

T_α (keV)	$C[T_i = (m_i/m_p)^a T_p] (10^{-8} \text{ cm}^3 \text{ s}^{-1})$				
	$a = 0$	$a = 0.25$	$a = 0.5$	$a = 0.75$	$a = 1.0$
5.44	1.0	1.1	1.3	1.5	1.9
8.16	1.7	1.9	2.1	2.4	2.9
10.88	2.3	2.5	2.8	3.2	3.7
16.32	3.5	3.7	4.1	4.5	5.0
21.76	4.3	4.6	5.0	5.5	6.1
27.20	5.1	5.3	5.8	6.3	6.9
32.64	5.7	6.0	6.5	7.0	7.7
43.52	6.8	7.2	7.7	8.2	8.9
54.40	6.7	6.9	8.5	9.1	9.4
65.28	8.3	8.7	9.2	9.7	10.1
76.16	8.9	9.2	9.6	10.0	10.4
87.04	9.3	9.6	10.0	10.2	10.6
97.92	9.6	9.9	10.3	10.6	10.9
108.80	9.9	10.3	10.4	10.8	11.1

TABLE 9
PHOTONS PER HYDROGEN ATOM ENTERING THE SHOCK IN SELECTED LINES

LINE	v_s								
	1000	1250	1500	1750	2000	2250	2500	2750	3000
FE = 0.0001									
He II.....	0.0117	0.0108	0.0102	0.0098	0.0094	0.0092	0.0091	0.0089	0.0088
C IV.....	0.0057	0.0067	0.0080	0.0096	0.0115	0.0138	0.0164	0.0192	0.0225
N V.....	0.0035	0.0043	0.0052	0.0063	0.0076	0.0090	0.0107	0.0125	0.0145
O VI.....	0.0185	0.0237	0.0298	0.0368	0.0447	0.0537	0.0635	0.0742	0.0861
FE = 0.0500									
He II.....	0.0090	0.0081	0.0075	0.0071	0.0069	0.0067	0.0067	0.0067	0.0067
C IV.....	0.0048	0.0057	0.0071	0.0092	0.0117	0.0149	0.0189	0.0236	0.0291
N V.....	0.0032	0.0039	0.0050	0.0059	0.0074	0.0093	0.0116	0.0143	0.0176
O VI.....	0.0190	0.0240	0.0302	0.0376	0.0462	0.0565	0.0692	0.0845	0.1026
FE = 0.1000									
He II.....	0.0078	0.0072	0.0068	0.0065	0.0065	0.0065	0.0065	0.0066	0.0067
C IV.....	0.0043	0.0052	0.0068	0.0094	0.0127	0.0167	0.0215	0.0274	0.0344
N V.....	0.0028	0.0040	0.0055	0.0066	0.0078	0.0101	0.0129	0.0164	0.0205
O VI.....	0.0163	0.0209	0.0270	0.0350	0.0456	0.0585	0.0746	0.0942	0.1178
FE = 0.1500									
He II.....	0.0072	0.0067	0.0065	0.0064	0.0064	0.0065	0.0065	0.0066	0.0068
C IV.....	0.0041	0.0049	0.0066	0.0097	0.0135	0.0179	0.0233	0.0299	0.0379
N V.....	0.0026	0.0045	0.0062	0.0068	0.0081	0.0107	0.0139	0.0179	0.0227
O VI.....	0.0159	0.0197	0.0260	0.0351	0.0469	0.0616	0.0800	0.1028	0.1308
FE = 0.2000									
He II.....	0.0070	0.0065	0.0064	0.0064	0.0064	0.0065	0.0066	0.0067	0.0068
C IV.....	0.0040	0.0047	0.0067	0.0100	0.0139	0.0186	0.0245	0.0317	0.0405
N V.....	0.0026	0.0049	0.0063	0.0069	0.0084	0.0112	0.0147	0.0191	0.0244
O VI.....	0.0161	0.0191	0.0258	0.0355	0.0482	0.0641	0.0844	0.1099	0.1412
FE = 0.2500									
He II.....	0.0067	0.0064	0.0063	0.0063	0.0064	0.0065	0.0066	0.0067	0.0069
C IV.....	0.0040	0.0047	0.0067	0.0098	0.0142	0.0192	0.0254	0.0330	0.0424
N V.....	0.0026	0.0049	0.0063	0.0077	0.0086	0.0115	0.0152	0.0200	0.0258
O VI.....	0.0164	0.0190	0.0258	0.0356	0.0492	0.0662	0.0879	0.1155	0.1501
FE = 0.3000									
He II.....	0.0070	0.0069	0.0068	0.0068	0.0067	0.0067	0.0067	0.0068	0.0069
C IV.....	0.0039	0.0054	0.0076	0.0106	0.0147	0.0199	0.0266	0.0348	0.0448
N V.....	0.0026	0.0033	0.0046	0.0064	0.0087	0.0119	0.0159	0.0210	0.0274
O VI.....	0.0166	0.0194	0.0264	0.0366	0.0503	0.0685	0.0921	0.1224	0.1606
FE = 0.4000									
He II.....	0.0069	0.0068	0.0068	0.0067	0.0067	0.0067	0.0068	0.0068	0.0069
C IV.....	0.0039	0.0053	0.0075	0.0107	0.0149	0.0204	0.0273	0.0359	0.0466
N V.....	0.0026	0.0033	0.0046	0.0064	0.0089	0.0122	0.0165	0.0220	0.0290
O VI.....	0.0176	0.0193	0.0265	0.0370	0.0516	0.0709	0.0966	0.1292	0.1717
FE = 0.5000									
He II.....	0.0069	0.0068	0.0067	0.0067	0.0067	0.0067	0.0068	0.0069	0.0070
C IV.....	0.0039	0.0052	0.0075	0.0106	0.0149	0.0204	0.0275	0.0364	0.0474
N V.....	0.0027	0.0032	0.0045	0.0064	0.0090	0.0124	0.0168	0.0225	0.0299
O VI.....	0.0186	0.0192	0.0264	0.0372	0.0521	0.0724	0.0993	0.1336	0.1790
FE = 0.6000									
He II.....	0.0069	0.0068	0.0067	0.0067	0.0067	0.0067	0.0068	0.0069	0.0070
C IV.....	0.0038	0.0051	0.0073	0.0105	0.0147	0.0203	0.0274	0.0364	0.0477
N V.....	0.0027	0.0032	0.0045	0.0064	0.0090	0.0124	0.0169	0.0228	0.0305
O VI.....	0.0194	0.0191	0.0262	0.0371	0.0523	0.0731	0.1007	0.1362	0.1836

TABLE 9—Continued

LINE	v_s								
	1000	1250	1500	1750	2000	2250	2500	2750	3000
FE = 0.7000									
He II.....	0.0068	0.0068	0.0067	0.0067	0.0067	0.0068	0.0068	0.0069	0.0071
C IV.....	0.0038	0.0050	0.0072	0.0103	0.0145	0.0201	0.0271	0.0362	0.0476
N V.....	0.0028	0.0031	0.0044	0.0063	0.0089	0.0123	0.0169	0.0229	0.0307
O VI.....	0.0201	0.0190	0.0260	0.0368	0.0520	0.0733	0.1009	0.1380	0.1862
FE = 0.8000									
He II.....	0.0068	0.0067	0.0067	0.0067	0.0068	0.0068	0.0068	0.0070	0.0071
C IV.....	0.0038	0.0049	0.0071	0.0101	0.0142	0.0196	0.0268	0.0358	0.0472
N V.....	0.0029	0.0031	0.0043	0.0062	0.0089	0.0123	0.0168	0.0228	0.0307
O VI.....	0.0201	0.0188	0.0257	0.0364	0.0517	0.0727	0.1011	0.1378	0.1872
FE = 0.9000									
He II.....	0.0068	0.0067	0.0067	0.0067	0.0068	0.0068	0.0069	0.0070	0.0071
C IV.....	0.0038	0.0048	0.0069	0.0098	0.0139	0.0193	0.0263	0.0353	0.0466
N V.....	0.0029	0.0030	0.0043	0.0061	0.0088	0.0122	0.0166	0.0227	0.0305
O VI.....	0.0207	0.0187	0.0254	0.0360	0.0512	0.0722	0.1007	0.1382	0.1863
FE = 1.0000									
He II.....	0.0068	0.0067	0.0067	0.0068	0.0068	0.0068	0.0069	0.0070	0.0072
C IV.....	0.0037	0.0047	0.0068	0.0096	0.0135	0.0187	0.0258	0.0347	0.0459
N V.....	0.0030	0.0030	0.0042	0.0060	0.0087	0.0122	0.0164	0.0224	0.0302
O VI.....	0.0211	0.0185	0.0251	0.0355	0.0505	0.0712	0.0999	0.1373	0.1854

NOTE.—FE = assumed fractional electron-ion equilibration.

(McLaughlin et al. 1996). A fine energy mesh was used to capture the resonance structure near threshold. The collision strengths at high energies were taken from the existing Coulomb-Born, Coulomb-Born-Oppenheimer, and Born approximations (Tully 1973; Golden et al. 1981; Clark, Sampson, & Goett 1982) and the complete energy range used to compute thermally averaged collision strengths. While these are the most sophisticated calculations available for excitation to the $n = 3$ levels, recent work at intermediate energies shows that continuum states must be included at impact energies above the ionization threshold (Bray et al. 1993). We anticipate that inclusion of the continuum states will *reduce* the He II excitation rates by roughly 20%. For the models here, to obtain the Balmer- α emission rates we add the excitation rates to the 3s and 3d levels to 0.12 times the excitation rate to 3p (88% of the 3p excitations producing 256 Å photons that escape). It is crucial to the results below that the excitation rates to 3s and 3d, which produce strong 1640 Å emission, decline relative to the ionization rate with increasing electron temperature, as indeed they must, being forbidden transitions.

3. SHOCK MODELS

We use numerical models of the evolution of electron temperature in the shocked gas, the evolution of the ionization states of the abundant elements, and the excitation to compute the UV line intensities. For a given shock velocity, we specify the preshock ionization state and temperature and the elemental abundances. A density of 0.06 atoms cm^{-3} is assumed, though in the limit that all radiation from He II and the Li-like ions is within the HUT slit, the various line intensity ratios are independent of this parameter. The set of models presented here assumes that hydrogen is $\frac{1}{2}$ ionized ahead of the shock, helium is neutral, carbon

is singly ionized, and oxygen and nitrogen are tied to hydrogen by charge transfer (Butler & Raymond 1980). The elemental abundances are taken to be H:He:C:N:O = 1.0:0.85:1.66 $\times 10^{-4}$:9.1 $\times 10^{-5}$:4.4 $\times 10^{-4}$, corresponding to a factor of 2 depletion of carbon in interstellar grains. The UV lines arise so close to the shock that there is inadequate time for any significant grain sputtering. However, gradual liberation of carbon will produce very faint, diffuse C IV emission far behind the shock (Vancura et al. 1994). The fractional heating of the electrons in the shock (T_e/T_i) is a model parameter. We specify also the degree of equilibration among the ion species. The models presented here are meant to match the HUT observations of SN 1006 (Raymond et al. 1995), so we set the thermal velocities of the ion species equal to that of hydrogen.

At the shock front, the total thermal energy is obtained from the jump conditions, and it is divided among protons, electrons, and other ions in accord with the equilibration parameters. The code follows the ion and electron temperature evolution by computing the exchange of energy between protons and electrons by Coulomb collisions (see, e.g., Spitzer 1978, p. 21) and the thermal energy loss by collisional ionization and excitation. The evolution of the postshock plasma is followed until the He II and Li-like ions are completely ionized. Then we compute the emission-line intensities. Table 9 presents ξ , the predicted line emission in photons per hydrogen atom (neutral or ionized) passing through the shock as a function of fractional equilibration (FE) for various shock velocities, v_s , between 1000 km s^{-1} and 3000 km s^{-1} . The absolute brightness of a face-on shock is then $\xi n_0 v_s / 4\pi$ photons $\text{cm}^{-2} \text{s}^{-1} \text{sr}^{-1}$. The intensities scale linearly with elemental abundance and with preshock density.

4. DISCUSSION

Table 10 presents the line intensities relative to C IV for a set of models chosen to match the 2350 km s⁻¹ H α line width observed in SN 1006 (Smith et al. 1991). (Note that the reddening corrected He II intensity in Table 1 of Raymond et al. 1995 should be 2.60 rather than the 2.40 listed.) The models with larger fractional equilibration require higher shock velocities because the thermal energy is shared between ions and electrons. The reddening-corrected line intensities observed by HUT are also given in Table 10. The reddening correction has little effect on the relative intensities except for that of O VI. The O VI line is also affected by the finite spatial extent of the HUT aperture for these measurements. In spite of the very wide (19") slit, Raymond et al. (1995) estimated that roughly half the O VI emission from the shock wave may have been outside the slit. (The exact fraction scales inversely with the preshock density, which is not very accurately known.) Therefore, the O VI intensity provides useful constraints only on the models for which the predicted value is smaller than that observed. Based on Table 10, a model with somewhat lower preshock density, $n_0 \sim 0.04$ cm⁻³, would match the data better, in that the O VI emission would be more spatially extended, and a smaller fraction of the total O VI photons would have fallen within the HUT aperture. The model value of $n_0 \sim 0.06$ cm⁻³ was based on the model calculations of Hamilton, Sarazin, & Szymkowiak (1986), but the recent discovery that much of the X-ray flux from SN 1006 is synchrotron emission (Willingale et al. 1996; Koyama et al. 1995) suggests that a smaller density might account for the thermal part of the emission.

From Table 10, it is apparent that the predicted N v:C IV ratio is similar to that observed, indicating that the assumed carbon depletion is reasonable. A slightly smaller depletion would fit the observations better, but the factor of 2 assumed is within the uncertainty. The other feature of Table 10 is that the best match for the He II:C IV ratio is achieved for very low values of the electron-ion equilibration: $T_e < 0.05T_i$. The fully equilibrated model differs from the observed value by about a factor of 4. CP predict $T_e \sim 0.20T_i$, but that model predicts less than $\frac{1}{2}$ the observed He II:C IV ratio. The discrepancy is about 3 times the 1 σ uncertainty in the measured value given by Raymond et al. (1995). Most of the theoretical uncertainty resides in the proton and alpha-particle excitation rates and in the assumed carbon depletion, both of which are rather hard to quantify. Considering these uncertainties, we probably cannot rule out the $T_e \sim 0.20T_i$ model, though a

smaller equilibration value agrees better with the observations. However, it is clear that we have rather firm evidence against complete equilibration in the nonradiative shocks of SN 1006. This is in contrast to what has been generally assumed in interpreting X-ray observations, where more rapid electron-ion equilibration has been favored (e.g., Willingale et al. 1996; see also discussion in Laming 1990).

This conclusion can be drawn principally because of the lines we observe in the far-UV; He II is excited by electrons, whereas excitation of the lower threshold Li-like transitions is dominated by protons and alpha particles. This result for the equilibration is basically consistent with analyses of the two-component H α profile from this and similar shocks (Smith et al. 1996). Analyses of optical and UV spectra of the much slower (~ 200 km s⁻¹) nonradiative shocks in the Cygnus Loop (Raymond et al. 1983; Long et al. 1992; Hester, Raymond, & Blair 1994) have proved to be ambiguous, but they are also consistent with weak heating of the electrons. At such low velocities, it might be expected that the mechanism of CP would break down, for the reasons given by Lesch (1990), i.e., that the reflected ion drift velocity will not be significantly greater than the ambient electron thermal velocity, and so rather little electron heating would be expected from the Buneman and ion-acoustic instabilities.

We are also rather uncertain about the direction of the magnetic field in the northwest filament. The morphology of SN 1006 and its position relative to the galactic plane suggest that we are looking at a quasi-parallel shock. However, a detailed examination of the situation must also account for the nonthermal X-rays seen on the northeast and southwest limbs (Koyama et al. 1995; Willingale et al. 1996) and evidence of a cosmic-ray precursor on the northwest limb (see Smith, Raymond, & Laming 1994). Such a discussion is beyond the scope of the present work, and it will be deferred to a later paper.

Returning to the primary point of this paper, our conclusion regarding the postshock equilibration permits us to narrow down considerably the allowed range for the shock velocity in SN 1006. In the limit of no equilibration, we would derive a shock velocity of 2480 ± 270 km s⁻¹ from the mean of the widths of the H α broad component (Smith et al. 1991) and the C IV $\lambda 1550$ line (Raymond et al. 1995), where the quoted errors for these measurements have been added in quadrature. (We neglect the He II $\lambda 1640$ width from Raymond et al. 1995 due to the large error quoted for it.) Taking the degree of equilibration to be $10\% \pm 10\%$, the

TABLE 10
PHOTON NUMBER RELATIVE TO C IV

ION	OBSERVED INTENSITY UNITS ^a	FE							
		0.0001 $v_s = 2250$	0.05 $v_s = 2250$	0.10 $v_s = 2250$	0.20 $v_s = 2500$	0.30 $v_s = 2500$	0.50 $v_s = 2750$	0.70 $v_s = 3000$	1.00 $v_s = 3000$
He II	0.62	0.67	0.45	0.39	0.27	0.25	0.19	0.15	0.16
C IV	1.00	1.00	1.00	1.00	1.00	1.00	1.00	1.00	1.00
N v	0.54	0.65	0.62	0.60	0.60	0.60	0.62	0.65	0.66
O VI	1.11 ^b	3.90	3.78	3.51	3.44	3.47	3.67	3.91	4.04

NOTE.—FE = assumed fractional electron-ion equilibration.

^a After reddening correction, from Raymond et al. (1995).

^b Observed O VI could be an underestimate, depending on unknown spatial distribution of O VI-emitting region compared with HUT aperture (see text).

shock velocity is increased to $2600 \pm 300 \text{ km s}^{-1}$. Combining this with the observed proper motion of $0'30 \pm 0'04 \text{ yr}^{-1}$ (Long et al. 1988) yields a distance to the remnant of $1.8 \pm 0.3 \text{ kpc}$, again with errors added in quadrature.

This new direct determination of the distance to SN 1006 based on the observed proper motion and derived velocity of the same filament has some immediate implications. With the observed angular size of $30'$, the diameter of the remnant must be $15.7 \pm 2.6 \text{ pc}$. With a known age of 1000 yr, this implies that the *mean* expansion velocity of the remnant has been $7850 \pm 1300 \text{ km s}^{-1}$. Historical analysis of the data on the supernova (as well as other circumstantial evidence) points toward a Type Ia supernova (see Minkowski 1966; Clark & Stephenson 1977; Schaefer 1996), and initial expansion velocities for Type Ia supernovae are often observed to be in excess of $10,000 \text{ km s}^{-1}$ (Jeffrey et al. 1992, and references therein). Hence, in principle, a mean velocity as high as we determine is not a problem.

Willingale et al. (1996) derive a shock velocity of $1400 \pm 200 \text{ km s}^{-1}$ and a distance of $700 \pm 100 \text{ pc}$. These results probably stem from the assumption in their analysis of complete electron-ion equilibration. Our larger shock velocity, distance, and corresponding remnant radius largely obviate the necessity these authors found to place observed absorption features of cold Fe with large widths ($\sim 8000 \text{ km s}^{-1}$) outside the remnant.

On another front, the thought of a Type Ia SN at a well-constrained distance has great potential interest to cosmologists. Over the last few years, the idea that SN Ia's are standard candles has undergone somewhat of a bad news-good new transformation. While an intrinsic spread in peak magnitudes has been identified, the spread is correlated with the speed of decline of the B light curve (Phillips 1993). The problem, of course, is that this SN was observed 1000 years ago, and only rough estimates on its peak visual magnitude are available ($V = -9.5$, Clark & Stephenson

1977; $V = -6 \pm 0.5$, Pskovskii 1978; $V = -4.9 \pm 0.5$, Schaefer 1996, for an average Type Ia light curve). Hence, it is difficult to use SN 1006 to constrain the peak magnitudes of Type Ia SNs.

If we turn the argument around instead, we can use current knowledge of SN Ia characteristics and estimate how bright the SN in 1006 A.D. might have been. Assuming our distance from above, a visual extinction to SN 1006 of $A_V = 0.31$ (see Raymond et al. 1995), and a mean absolute peak visual magnitude for SN Ia's of $M_V = -18.23 \pm 0.28$ from Phillips (1993), we find a posteriori that SN 1006 should have had a peak visual magnitude of -6.6 ± 0.6 . This value is consistent with Pskovskii's (1978) estimate, and also possibly with the more recent work of Schaefer (1996), depending on which of his Type Ia light curve templates is considered. The peak magnitude estimated by Clark & Stephenson (1977) would imply a peak absolute magnitude of -20.1 , roughly a magnitude brighter than the brightest SN Ia with a reliable distance (see Phillips 1993).

In conclusion, then, we have new determinations for the shock velocity, distance, and radius of SN 1006. These are considerably more precise than was previously possible due to our improved knowledge of the electron-ion equilibration behind the shock. An accurate comparison with plasma simulations, however, must await a thorough examination of morphology of SN 1006 in order to determine the magnetic field geometry.

J. M. L. is grateful to Peter Cargill for helpful discussions on plasma instabilities, and to Uri Feldman for continuing support. This work was also supported by NASA contract NAS 5-27000 to J. H. U. and NASA grant NAG 8-1074 to S. A. O. Also B. M. McL. thanks the Minnesota Supercomputer Institute for the generous support of computing resources on the Cray Y-MP-C916/9P/512 Mw. We also thank Richard Willingale, the referee, for a careful reading of the manuscript.

REFERENCES

- Aggarwal, K. M., Callaway, J., Kingston, A. E., & Unnikrishnan, K. 1992, *ApJS*, 80, 473
- Alder, K., Bohr, A., Huus, T., Mottelson, B., & Winther, A. 1956, *Rev. Mod. Phys.*, 28, 432
- Arnaud, M., & Rothenflug, R. 1985, *A&AS*, 60, 435
- Berrington, K. A., Kisielius, R., & Norrington, P. H. 1996, *A&A*, in press
- Bray, I., McCarthy, I. E., Wigley, J., & Stelbovics, A. T. 1993, *J. Phys. B*, 26, L831
- Briggs, J. S., & Dubé, L. J. 1980, *J. Phys. B*, 13, 771
- Buneman, O. 1958, *Phys. Rev.*, 115, 503
- Burgess, A. 1974, *J. Phys. B*, 7, L364
- Burgess, A., Hummer, D. G., & Tully, J. A. 1970, *Philos. Trans. R. Soc. London*, A266, 225 (BHT)
- Butler, S. E., & Raymond, J. C. 1980, *ApJ*, 240, 680
- Cargill, P. J., & Papadopoulos, K. 1988, *ApJ*, 329, L29 (CP)
- Chevalier, R. A., Kirshner, R. P., & Raymond, J. C. 1980, *ApJ*, 235, 186
- Clark, D. H., & Stephenson, F. R. 1977, *The Historical Supernovae* (Oxford: Pergamon Press)
- Clark, R. E. H., Sampson, D. H., & Goett, S. J. 1982, *ApJS*, 49, 545
- Crandall, D. H., Phaneuf, R. A., Hasselquist, B. E., & Gregory, D. C. 1979, *J. Phys. B*, 12, L249
- Dubé, L. J., & Briggs, J. S. 1981, *J. Phys. B*, 14, 4595
- Forslund, D. W., Quest, K. B., Brackbill, J. U., & Lee, K. 1984, *J. Geophys. Res.*, 89, 2142
- Golden, L. B., Clark, R. E. H., Goett, S. J., & Sampson, D. H. 1981, *ApJS*, 45, 603
- Hamilton, A. J. S., Sarazin, C. L., & Szymkowiak, A. E. 1986, *ApJ*, 300, 698
- Hatton, G. J., Lane, N. F., & Winter, T. G. 1979, *J. Phys. B*, 12, L571
- Hester, J. J., Raymond, J. C., & Blair, W. P. 1994, *ApJ*, 420, 721
- Hose, G. 1995, *Phys. Rev. A*, 51, 2222
- Jeffrey, D. J., Leibundgut, B., Kirshner, R. P., Benetti, S., Branch, D., & Sonneborn, G. 1992, *ApJ*, 397, 304
- Koyama, K., Petre, R., Gotthelf, E. V., Hwang, U., Matsuura, M., Ozaki, M., & Holt, S. S. 1995, *Nature*, 378, 255
- Laming, J. M. 1990, *ApJ*, 362, 219
- Lesch, H. 1990, *A&A*, 239, 437
- Long, K. S., Blair, W. P., Vancura, O., Bowers, C. W., Davidsen, A. F., & Raymond, J. C. 1992, *ApJ*, 400, 214
- Long, K. S., Blair, W. P., & van den Bergh, S. 1988, *ApJ*, 333, 749
- Magee, N. H., Jr., Mann, J. B., Merts, A. L., & Robb, W. D. 1977, *Los Alamos Informal Report LA-6691-MS*
- McLaughlin, B. M., Gillan, C. J., Raymond, J. C., & Dahler, J. S. 1996, in preparation
- Minkowski, R. 1966, *AJ*, 71, 371
- Phillips, M. M. 1993, *ApJ*, 413, L105
- Pskovskii, Y. P. 1978, *Soviet Astron.*, 22, 420
- Quest, K. B., Forslund, D. W., Brackbill, J. U., & Lee, K. 1983, *Geophys. Res. Lett.*, 10, 471
- Raymond, J. C., Blair, W. P., Fesen, R. A., & Gull, T. R. 1983, *ApJ*, 275, 636
- Raymond, J. C., Blair, W. P., & Long, K. S. 1995, *ApJ*, 454, L31
- Schaefer, B. E. 1996, *ApJ*, 459, 438
- Scudder, J. D., Mangeny, A., Lacombe, C., Harvey, C. C., & Aggson, T. L. 1986b, *J. Geophys. Res.*, 91, 11053
- Scudder, J. D., et al. 1986a, *J. Geophys. Res.*, 91, 11019
- Scudder, J. D., Mangeny, A., Lacombe, C., Harvey, C. C., Wu, C. S., & Anderson, R. R. 1986c, *J. Geophys. Res.*, 91, 11075
- Seaton, M. J. 1964, *MNRAS*, 127, 191
- Smith, R. C., Kirshner, R. P., Blair, W. P., & Winkler, P. F. 1991, *ApJ*, 375, 652
- Smith, R. C., Laming, J. M., & Raymond, J. C. 1996, in preparation
- Smith, R. C., Raymond, J. C., & Laming, J. M. 1994, *ApJ*, 420, 286
- Spitzer, L., Jr. 1978, *Physical Processes in the Interstellar Medium* (New York: Wiley & Sons)
- Tully, J. A. 1973, *Canadian J. Phys.*, 51, 2047
- Vancura, O., Raymond, J. C., Dwek, E., Blair, W. P., Long, K. S., & Foster, S. 1994, *ApJ*, 431, 188
- Walling, R. S., & Weisheit, J. C. 1988, *Phys. Rep.*, 162, 1
- Willingale, R., West, R. G., Pye, J. P., & Stewart, G. C. 1996, *MNRAS*, 278, 749
- Zygelman, B., & Dalgarno, A. 1987, *Phys. Rev. A*, 35, 4085